University of Thi-Qar Journal of Science (UTJsci)
E-ISSN: 2709-0256, P-ISSN: 1991-8690, Vol. 11, No. 2, Dec. 2024

Three-Layers Slab Waveguide with Chiral Metamaterial Core and Graphene Interfaces

Hawraa H. Salman*[1a] and Hassan A. Yasser[2b]

[1] *Department of Physics, Education College for Pure Science, University of Thi-Qar, Thi-Qar, Iraq.*
[2]*Department of Physics, College of Science, University of Thi-Qar, Thi-Qar, Iraq.*

[b]E-mail: hassan.yasser@sci.utq.edu.iq
[a*]Corresponding author: hawraa_ham.ph@utq.edu.iq

Received: 2024-05-21, Revised: 2024-06-06, Accepted: 2024-06-11, Published: 2024-12-05

***Abstract*—We investigate the dispersion relation of guided waves in a three-layered slab waveguide, with one layer filled with chiral metamaterial and the other two filled with normal materials. This waveguide model contains an interface between adjacent layers. Graphene was used for this purpose due to its excellent optical properties. The interface thickness is** $1.02nm$ **, where three monolayer graphene was used. Propagation equations and special cases for this type of structure and graphene properties were obtained. Such phenomena have also been given physical explanations. Our theoretical work has been validated by simulation findings. These chiral structures have potential uses in millimeter-wave and microwave-integrated circuits.**

***Keywords*—Chiral metamaterial, Slab waveguide, Graphene.**

I. INTRODUCTION

The study of electromagnetic wave properties of dielectric materials is an essential element in which electromagnetic waves are used to transport energy from one place to another. Electromagnetic waveguides are specifically engineered electromagnetic structures or media that facilitate the effective flow of energy or information in a certain direction. The waveguide is a structure that uses total internal reflection to both confine and direct the wave beam [1] Because of the well-known phenomenon of optical activity chiral media have been known for a very long time in the optical region. Two intrinsic eigenwaves with left- and right-handed circular polarizations, as well as different phase velocities and refraction indices, are the defining characteristics of these media [2]. Since chirality (coupling) parameters can be appropriately controlled to produce negative reflection and/or refraction, chiral metamaterials have also attracted interest [3]. In this paper, we have analyzed the dispersion relation of even and odd modes for both right-hand circularly polarized waves (RCP) and left-hand circularly polarized waves (LCP) and graphene properties in a three-layered waveguide, where cladding layers are covered by the normal materials and the central layer are occupied by chiral left-handed material with graphene interfaces.

II.WAVE EQUATION IN SLAB WAVEGUIDE

In this work, there are two types of materials: the non-chiral type and the chiral type. In the following subsections, we will try to clarify the wave equation in both cases.

A. Non-Chiral Media

The expression for the two constitutive relations that characterize the medium's reaction to applied fields is

$$\vec{D} = \varepsilon \vec{E} \quad , \; \vec{B} = \mu \vec{H} \tag{1}$$

where $\vec{E}$, $\vec{H}$, $\vec{D}$, and $\vec{B}$ are the electric field, magnetic field, electric displacement, and magnetic flux density, respectively. Here, the permittivity ε and permeability μ are scalars for isotropic medium. Using some of the facts, the wave equation for the longitudinal component of the electric field will be [4].

$$\frac{\partial^2 E_z}{\partial x^2} + \left[k_i^2 - \beta^2 \right] E_z = 0 \quad , \; i = \text{layer index} \tag{2}$$

where $k_i = k_0 \sqrt{\varepsilon_i \, \mu_i}$, $\beta = k_0 n_{eff}$ is the propagation constant along the longitudinal direction, k_0 is the free space wave number, and n_{eff} is the modal effective refractive index. The wave equation for the longitudinal component of the magnetic field will be [5]

$$\frac{\partial^2 H_z}{\partial x^2} + \left[k_i^2 - \beta^2 \right] H_z = 0 \quad , \; i = \text{layer index} \tag{3}$$

It should be noted that the magnetic and electric fields' longitudinal components are independent.

B. Chiral Media

The electric and magnetic fields in chiral media are connected as [6].

$$\vec{D} = \vec{\varepsilon} \vec{E} - iK \sqrt{\varepsilon \mu} \hat{z} \hat{z} \cdot \vec{H} \tag{4a}$$

$$\vec{B} = \vec{\mu} \vec{H} + iK \sqrt{\varepsilon \mu} \hat{z} \hat{z} \cdot \vec{E} \tag{4b}$$

https://doi.org/10.32792/utq/utjsci/v11i2.1254

where K represents the chirality factor and $\hat{z}\hat{z}$ is a dyadic tensor. Note that the second term in Eqs. (4) represents the coupling due to chirality. We shall be content to mention the coupled wave equations to the electric and magnetic fields here as deriving the wave equation here necessitates working on vectorial Maxwell's equations, which is time-consuming and complex and takes us outside the topic of the research [7].

$$\frac{\partial^2 E_z}{\partial x^2} + q^2 (E_z - iK\sqrt{\frac{\mu}{\varepsilon}} H_z) = 0 \qquad (5a)$$

$$\frac{\partial^2 H_z}{\partial x^2} + q^2 (H_z + iK\sqrt{\frac{\varepsilon}{\mu}} E_z) = 0 \qquad (5b)$$

where $q^2 = w^2 \varepsilon \mu - \beta^2$. Note that, Eqs.(5) shows that the two longitudinal fields are coupled by the chirality. Consequently, the fields are typically hybrid rather than *TE* or *TM* modes as in the case of zero chirality, where $K = 0$. The expression for electromagnetic fields in a chiral medium is [8]:

$$E_z = E_{z+} + E_{z-} \qquad (6a)$$

$$H_z = H_{z+} + H_{z-} \qquad (6b)$$

The relationship between the magnetic and electric fields is established by

$$H_{z\pm} = \pm j\, E_{z\pm}/\eta \qquad (7)$$

where $\eta = \sqrt{\mu/\varepsilon}$ is the intrinsic impedance of the medium.

III. MODAL DESCRIPTION

The structure shown in Fig.1 consists of the chiral-guided film surrounded by a normal material with parameters ε_1 and μ_1. The surrounding medium is assumed to exhibit no chirality. The central layer (Region 2) is located in the region at $-d/2 \le x \le d/2$ with isotropic chiral negative index metamaterial that has a permittivity ε_2, permeability μ_2, chirality parameter K_2 and thickness d, while the cover layer (Region 1) is located at $x \ge d/2$ and the substrate layer (Region 3) is located in the region $x \le -d/2$.

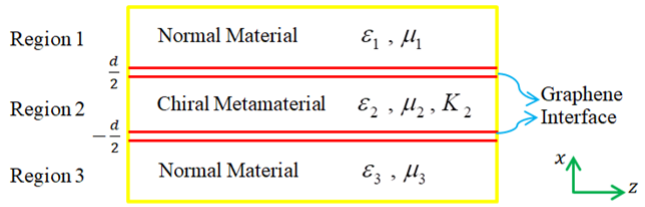

Fig. 1: Schematic of slab waveguide having chiral metamaterial in core layer with graphene interfaces

IV. THEORETICAL INVESTIGATION

Assuming that the electromagnetic wave propagates in a z-direction with harmonic time fields, the fields can take the form $E_o e^{i(\beta z - wt)}$. Attention that, in our derivations, the method of the paper [9] will be used, and the necessary adjustments will be made to include the changes adopted in this work. The reason for using this method is to separate the results based on odd and even including RCP and LCP.

A. *Dispersion Relation of Even Modes*

In this model, the chiral metamaterial is at the core region only. For even modes, the solutions of Eqs.(2) at non-chiral layers and (5a) at the chiral layer (where Eqs.(6a) will use to solve (5a)) are

$$E_{z1} = A\, e^{-q_1(x-h)} \quad , \quad x \ge h \qquad (8a)$$

$$E_{z2} = \underbrace{B \cos q_{2+} x}_{E_{z2+}} + \underbrace{C \cos q_{2-} x}_{E_{z2-}} \quad , -h \le x \le h \qquad (8b)$$

$$E_{z3} = A\, e^{q_1(x+h)} \quad , \; x \le -h \qquad (8c)$$

where $h = d/2$ and

$$q_{2\pm} = \sqrt{k_{2\pm}^2 - \beta^2}, \quad q_i = \sqrt{\beta^2 - k_i^2} \quad , \quad i = 1,3 \qquad (9)$$

The parameters A, B, C, and D represent the amplitudes of the waves in the different layers. Using Eqs.(6b) and (7) to find H_{z2} and Eq.(3) to find H_{z1} and H_{z3}, the longitudinal magnetic fields in the three layers will be

$$H_{z1} = D\, e^{-q_1(x-h)} \quad , \; x \ge h \qquad (10a)$$

$$H_{z2} = \frac{i}{\eta_2}[B \cos q_{2+} x - C \cos q_{2-} x \,] \quad , -h \le x \le h \qquad (10b)$$

$$H_{z3} = D\, e^{q_1(x+h)} \quad , \; x \le -h \qquad (10c)$$

The longitudinal and transverse components of magnetic and electric fields E_y , H_y are connected [9]

$$E_y = \frac{ik\eta}{q^2} H_z' \qquad (11a)$$

$$H_y = -\frac{ik}{q^2 \eta} E_z' \qquad (11b)$$

where the prime refers to the derivation with respect to x. Using Eqs.(10) and (11a), yields

$$E_{y1} = \frac{ik_1\eta_1}{q_1} D\, e^{-q_1(x-h)} \qquad (12a)$$

$$E_{y2} = \frac{-k_{2+}}{q_{2+}} B \sin q_{2+} x + \frac{k_{2-}}{q_{2-}} C \sin q_{2-} x \qquad (12b)$$

$$E_{y3} = \frac{-ik_1\eta_1}{q_1} D e^{q_1(x+h)} \qquad (12c)$$

Using Eq.(10) and (11b), yields

$$H_{y1} = \frac{-ik_1}{q_1\eta_1} A\, e^{-q_1(x-h)} \quad (13a)$$

$$H_{y2} = \frac{-ik_{2+}}{q_{2+}\eta_2} B \sin q_{2+}x - \frac{ik_{2-}}{q_{2-}\eta_2} C \sin q_{2-}x \quad (13b)$$

$$H_{y3} = \frac{ik_1}{q_1\eta_1} A\, e^{q_1(x+h)} \quad (13c)$$

where η_1, η_2 are the intrinsic impedance of the cladding and central regions, respectively. The following conditions apply to the waves that are transferred over the interfaces [10]

$$E_{zi} = E_{zj}\ ,\ H_{zi} - H_{zj} = -\sigma E_{yi} \quad (14a)$$

$$E_{yi} = E_{yj}\ ,\ H_{yi} - H_{yj} = \sigma E_{zi} \quad (14b)$$

Applying these boundary conditions at the $x = \pm h$ on the indicated fields, we get

$$A - B\ \cos q_{2+}h - C\ \cos q_{2-}h = 0 \quad (15a)$$

$$B\ \cos q_{2+}h - C\ \cos q_{2-}h + ir_1\eta_2\ D = 0 \quad (15b)$$

$$m_1\, B\, X\ \cos q_{2+}h - m_2\ CY\ \cos q_{2-}h + i\,\eta_1 D = 0 \quad (15c)$$

$$\eta_2 r_2 A - m_1\eta_1\, BX\ \cos q_{2+}h - m_2\,\eta_1\, CY\ \cos q_{2-}h = 0 \quad (15d)$$

where

$$m_1 = \frac{k_{2+}\, q_1}{k_1\, q_{2+}}\ ,\ m_2 = \frac{k_{2-}\, q_1}{k_1\, q_{2-}}\ ,\ r_1 = 1 - i\,\frac{\sigma\, k_1\eta_1}{q_1}\ ,$$

$$r_2 = 1 + i\,\frac{\sigma\, q_1\eta_1}{k_1},\ X = \tan q_{2+}h\ ,\ Y = \tan q_{2-}h$$

Here, to facilitate the solutions, we united all the functions to *cos* function using the assumptions $\sin q_{2+}h = X\ \cos q_{2+}h$ and $\sin q_{2-}h = Y\ \cos q_{2-}h$. The determinant of coefficients in Eqs.(15) may be written as

$$\begin{vmatrix} 1 & -\cos q_{2+}h & -\cos q_{2-}h & 0 \\ 0 & \cos q_{2+}h & -\cos q_{2-}h & ir_1\eta_2 \\ 0 & m_1 X\ \cos q_{2+}h & -m_2 Y\ \cos q_{2-}h & i\,\eta_1 \\ \eta_2 r_2 & -m_1\eta_1 X\ \cos q_{2+}h & -m_2\eta_1 Y\ \cos q_{2-}h & 0 \end{vmatrix} = 0 \quad (16)$$

A non-trivial solution of the system in Eq.(15) can exist only if the determinant of coefficients in Eq.(16) vanishes. Any known mathematical method can be used to determine this determinant, which will lead to the simplified formula of the dispersion relation

$$i\,\eta_1^2 (m_1 X + m_2 Y) - 2ir_1\eta_1\eta_2 m_1 m_2 XY - 2ir_2\eta_1\eta_2 + ir_1 r_2\eta_2^2 (m_1 X + m_2 Y) = 0 \quad (17)$$

Substituting the definitions of m_1, m_2 and carrying many simplifications, Eq.(17) may be rewritten as

$$\left[\frac{r_2 k_1}{\eta_1 q_1} + \frac{\rho k_{2+} X}{\eta_2 q_{2+}}\right]\left[\frac{\eta_1 k_1}{q_1} + \frac{\rho r_1\eta_2 k_{2-} Y}{q_{2-}}\right] + \left[\frac{r_2\eta_1 k_1}{q_1} + \frac{\rho r_1 r_2\eta_2 k_{2+} X}{q_{2+}}\right]\left[\frac{k_1}{\eta_1 q_1} + \frac{\rho k_{2-} Y}{r_2\eta_2 q_{2-}}\right] = 0 \quad (18)$$

The dispersion relation of the even modes (RCP and LCP) in a symmetric slab waveguide with a chiral metamaterial core is represented by above equation.

B. Dispersion Relation of Odd Modes

The longitudinal field solutions in the three-layers for odd modes are given by

$$E_{z1} = A\, e^{-q_1(x-h)} \quad , x \ge h \quad (19a)$$

$$E_{z2} = B \sin q_{2+}x + C \sin q_{2-}x \quad , -h \le x \le h \quad (19b)$$

$$E_{z3} = -Ae^{q_1(x+h)} \quad , x \le -h \quad (19c)$$

and

$$H_{z1} = D\, e^{-q_1(x-h)} \quad , x \ge h \quad (20a)$$

$$H_{z2} = \frac{i}{\eta_2}[B \sin q_{2+}x - C \sin q_{2-}x\ ] \quad , -h \le x \le h \quad (20b)$$

$$H_{z3} = -De^{q_1(x+h)} \quad , x \le -h \quad (20c)$$

The coefficients equations system will be operated in a similar way as in the even modes

$$A - B\ \sin q_{2+}h - C \sin q_{2-}h = 0 \quad (21a)$$

$$B\ \sin q_{2+}h - C \sin q_{2-}h + ir_1\eta_2\ D = 0 \quad (21b)$$

$$-m_1\, XB \sin q_{2+}h + m_2 Y\ C \sin q_{2-}h + i\,\eta_1 D = 0 \quad (21c)$$

$$\eta_2 r_2 A + m_1\eta_1\, XB\ \sin q_{2+}h + m_2\,\eta_1 Y\ C \sin q_{2-}h = 0 \quad (21d)$$

Here, we united all the functions to *sin* function using the assumptions $\cos q_{2+}h = X\ \sin q_{2+}h$ and $\cos q_{2-}h = Y\ \sin q_{2-}h$. The determinant of coefficients in Eqs.(21) must be zero. That is,

$$\begin{vmatrix} 1 & -\sin q_{2+}h & -\sin q_{2-}h & 0 \\ 0 & \sin q_{2+}h & -\sin q_{2-}h & ir_1\eta_2 \\ 0 & -m_1 X \sin q_{2+}h & m_2 Y \sin q_{2-}h & i\,\eta_1 \\ \eta_2 r_2 & m_1\eta_1 X \sin q_{2+}h & m_2\eta_1 Y \sin q_{2-}h & 0 \end{vmatrix} = 0 \quad (22)$$

By applying any mathematical method to calculate the determinant and simplifying the resultant, we obtain the simplified formula

$$\left[\frac{r_2 k_1}{\eta_1 q_1} + \frac{\rho k_{2+}}{\eta_2 q_{2+}} X\right]\left[\frac{\eta_1 k_1}{q_1} + \frac{\rho r_1\eta_2 k_{2-}}{q_{2-}} Y\right] + \left[\frac{r_2\eta_1 k_1}{q_1} + \frac{\rho r_1 r_2\eta_2 k_{2+}}{q_{2+}} X\right]\left[\frac{k_1}{\eta_1 q_1} + \frac{\rho k_{2-}}{r_2\eta_2 q_{2-}} Y\right] = 0 \quad (23)$$

where $X = \cot q_{2+}h$, $Y = \cot q_{2-}h$. Note that, Eqs.(18) and (23) are the same except for the difference in the value of ρ , which represent the dispersion relations of even and odd modes, respectively. Moreover, the signs $(+,-)$ at the sub-index refer to the RCP and LCP, respectively.

C. Generalized Dispersion Relation

For even modes, the RCP and LCP can be found in Eq.(18), where the RCP mode is found by taking $X \ne 0$

and $Y=0$, while the LCP is found by setting $X=0$ and $Y\neq 0$. Also, the odd modes can be found in Eq.(23), where the RCP and LCP can be found by taking $X\neq 0$ and $Y=0$ for the RCP, while the LCP is found by setting $X=0$ and $Y\neq 0$. In general, from the above assumptions, we get four equations. Two equations for the even modes are for the cases RCP and LCP and the same for the odd modes. All these equations can be combined in a generalized formula for slab waveguide has a chiral metamaterial layer in the core and a sheet of graphene on the interfaces as

$$q_{2\pm}h=\tan^{-1}\left[\frac{-\rho}{2r_2}\frac{k_{2\pm}}{q_{2\pm}}\frac{q_1}{k_1}\frac{\eta_1^2+r_1r_2\eta_2^2}{\eta_1\eta_2}\right]^{\rho}+m\pi \quad (24)$$

where m is the mode order of the hybrid H_m mode. Here it must be emphasized that, the symbol $\rho=(+,-)$ refer to the odd and even modes. Without chirality and graphene interfaces, we have

$$r_1=r_2=1,\ q_{2\pm}=q_2,\ k_1=k_0n_1,\ k_2=k_0n_2$$

$$q_1=k_0\sqrt{n_{eff}^2-n_1^2},\quad q_2=k_0\sqrt{n_2^2-n_{eff}^2}$$

such that the dispersion relation will be

$$q_2h=\tan^{-1}\left[-\frac{\rho}{2}\frac{n_2q_1}{n_1q_2}\frac{\eta_1^2+\eta_2^2}{\eta_1\eta_2}\right]^{\rho}+m\pi\ ,\ m=0,1,..\ (25)$$

The last equation is well known in scientific research [4,5], producing the *TM* mode for a three-layer slab metamaterial waveguide.

For nihility chiral metamaterial media and no graphene interfaces, where $\varepsilon_2=0$, $\mu_2=0$, the parameters will be $r_1=r_2=1,\ q_{2+}=q_{2-}=q_2,\ k_1=k_0n_1,\ k_{2\pm}=\pm k_0K_2$. Such that the dispersion relation takes the formula

$$q_2h=\pm\tan^{-1}\left[-\rho\frac{q_1K_2}{q_2n_1}\right]^{\rho}+m\pi \quad (26)$$

Note that, here, the signs $(+,-)$ represent the RCP and LCP modes, respectively.

V. GRAPHENE PROPERTIES

Because of its exceptional optical characteristics, high carrier mobility, and flexibility, graphene (a monolayer of carbon atoms arranged in a honeycomb lattice) is one of the best materials for optoelectronic devices and nanoelectronics. In particular, graphene's surface conductivity may be constantly adjusted in the terahertz band by applying the chemical potential through an external gate voltage [11]. Graphene's relative permittivity is

$$\varepsilon_g=1-\frac{j\sigma}{w\,\varepsilon_0\Delta} \quad (27)$$

in which $\Delta=0.34nm$ is graphene sheet thickness. The graphene complex refractive index can be expressed as $n_g=\sqrt{\varepsilon_g}$. The thickness and conductivity of a five-layer graphene can be computed by considering $\sigma\to 5\sigma$ and $\Delta\to 5\Delta$. With a thickness significantly less than the excitation wavelength, the bulk conductivity and surface conductivity are correlated by $\sigma_V=\sigma/\Delta$ [12,13]. The Kubo formula can be used to determine graphene's surface conductivity

$$\sigma=\frac{ie^2k_BT}{\pi\hbar^2\left(w+i\tau^{-1}\right)}\left[\frac{E_F}{k_BT}+2\ln\left(1+e^{\frac{-E_F}{k_BT}}\right)\right]+\frac{i\,e^2}{4\pi\hbar}\ln\left[\frac{2|E_F|-\hbar(w+i\tau^{-1})}{2|E_F|+\hbar(w+i\tau^{-1})}\right] \quad (28)$$

where e is the charge of an electron, E_F is the Fermi energy (or chemical potential) of graphene, which can be controlled by applying bias voltage or chemical doping, $\tau=1/2\Gamma$ is the momentum relaxation time with Γ is the scattering rate, T is the Kelvin temperature, k_B is Boltzmann's constant and $\hbar$ is the reduced Plank's constant [11]. Electromagnetic waves bonded to the metal-dielectric interface are called surface plasmons. When the real component of the dielectric constant is negative, and the imaginary part is very small compared to the negative real part, a material is said to be plasmonic in order to achieve minimal losses. This demonstrates how the chemical potential and input excitation frequencies of graphene have a significant influence on its plasmonic behavior. Understanding the propagating surface plasmon (SPP) and localized surface plasmon (LSP) on graphene requires an understanding of the interaction of light with the surface [14,15].

VI. RESULTS AND DISCUSSION

In this section, we will take a three-layer graphene interface with a thickness $1.02nm$ and $v_F=1\times10^6\,m/s$ is the Fermi velocity and $m_o=8\times10^4cm^2/sV$ is the carrier mobility parameter and $T=300K^o$ to simulate the properties of graphene material. Other parameters will be imposed during the simulation.

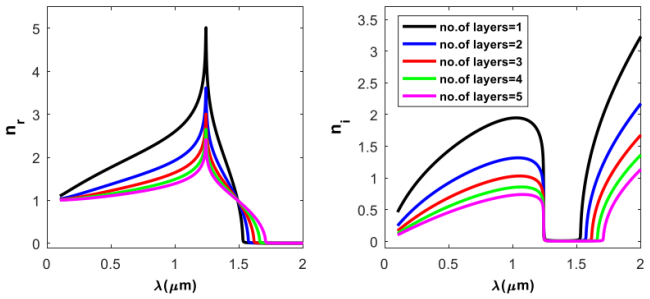

Fig. 2: Real and imaginary parts of refractive index as functions of wavelengths for number of layers at $E_F=0.5eV$.

Fig.2 shows real and imaginary parts of the refractive index of graphene as a function of wavelength for the number of graphene layers at the chemical potential $E_F=0.5eV$. This is in order to clarify the effect of increasing wavelength on the graphene properties when a certain chemical potential is used. The real part of the refractive index has a nonlinear increase that is inversely proportional to the number of graphene layers, and then it drops to zero. The lines farther from the left turn to be closer

after passing point (1,1.5). The imaginary part of the refractive index shows a nonlinear increase within a range $\lambda = (0-1.3)\,\mu m$, then a decrease starting at $\lambda = 1.3\,\mu m$. Finally, the large increase in the imaginary part is at a wavelength greater than $1.5\ \mu m$.

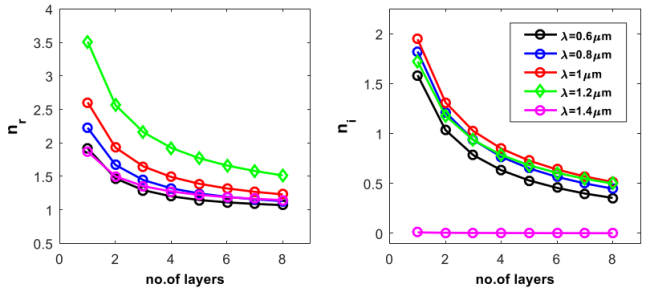

Fig. 3: Real and imaginary parts of refractive index as functions of number of layers for many wavelengths at $E_F = 0.5eV$.

Fig.3 represents real and imaginary parts of the refractive index as a function of the number of graphene layers for different wavelengths at the chemical potential $E_F = 0.5eV$. Note a clear decrease for the real and imaginary parts of the refractive index with an increase in the number of layers despite the different wavelengths. In general, for a single layer, the real part takes the highest value compared to the imaginary part of the refractive index. It is worth mentioning that the number of layers refers to the thickness; therefore, controlling of the number of layers (decrease or increase) provides flexibility to control the thickness of the graphene interface. As a result, it can be said that the refractive index for multilayered graphene decreases with increased thickness.

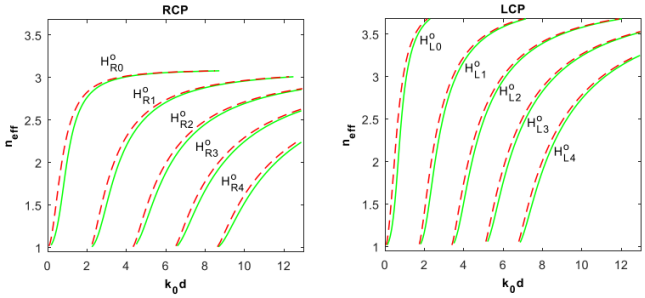

Fig. 4: Dispersion relation for odd modes, where the green and red lines represent the case $\sigma = 0$ and $\sigma \neq 0$, respectively.

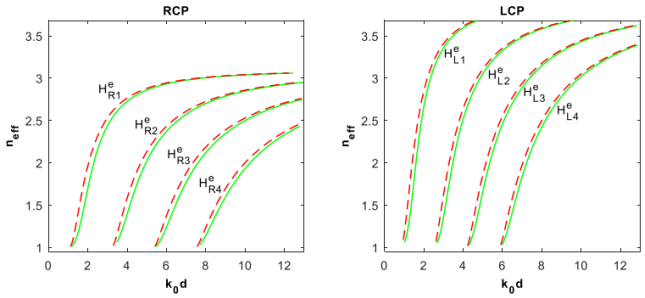

Fig. 5: Dispersion relation for even modes, where the green and red lines represent the case $\sigma = 0$ and $\sigma \neq 0$, respectively.

Figs.4 and 5 illustrate dispersion relations for odd and even modes, respectively. The green color refers to the case of $\sigma = 0$ while the red color represents the $\sigma \neq 0$ case. The parameters used to get these figures are: $K_1 = 0,\ K_2 = 0.4,\ \varepsilon_1 = \mu_1 = 1,\ \varepsilon_2 = \mu_2 = -3.5$ and $E_F = 1\times10^{-6}eV$. Here, the thickness of the guided layer is $d = 1\mu m$. We note that modes in case $\sigma \neq 0$ appears first and then comes after modes in the case of $\sigma = 0$. As a result, we can get the same value for effective refractive index n_{eff} within the less normalized frequency $k_o d$ in the presence of graphene interfaces case. Compared with the case RCP, the effective refractive index n_{eff} in the LCP case has great values, also LCP modes appear within the lower normalized frequency range. All modes begin at $n_{eff} = 1$ with a backward propagation and turn into a forward propagation when increasing normalized frequency. The propagation characteristics of light in the waveguide depend on the frequency of the light. In metamaterial waveguide with graphene, there can be a critical $k_o d$ value. Below this value, the light propagates backward. However, as $k_o d$ increases beyond this critical point, the light starts forward propagation. Backward propagation is due to the presence of metamaterials, but this change in behavior occurs due to the influence of graphene with increasing normalized frequency.

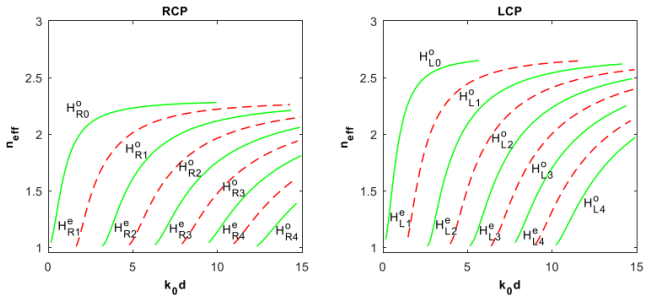

Fig. 6: Dispersion relation at $\varepsilon_2 = \mu_2 = -2.5$, where the green and red lines represent the case odd and even modes, respectively.

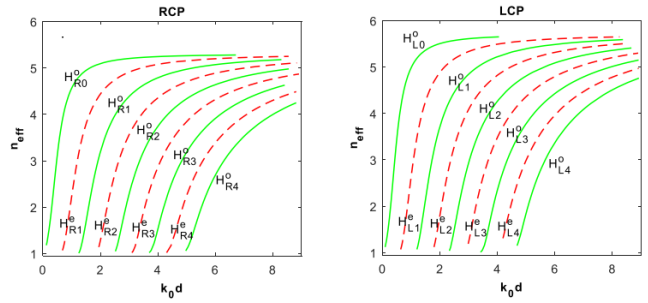

Fig. 7: Dispersion relation at $\varepsilon_2 = \mu_2 = -5.5$, where the green and red lines represent the case odd and even modes, respectively.

Figs.6 and 7 show the dispersion relations for guiding modes at different values for the dielectric constants in the core region in waveguide structure. The green lines refer to the odd modes. While the red lines represent the even modes. The thickness of the central layer in the waveguide is $d = 4\mu m$ either the other parameters are: $K_1 = 0,\ K_2 = 0.2,\ \varepsilon_1 = \mu_1 = 1$ and $E_F = 1eV$. Here, the figures are in the case of the use of graphene interfaces, which means $\sigma \neq 0$. The dielectric constants are $\varepsilon_2 = \mu_2 = -2.5$ in Fig.6 and $\varepsilon_2 = \mu_2 = -5.5$ in Fig.7. Note from Fig.6, the modes RCP appears within the range of the effective refractive index $n_{eff} < 2.5$ and $k_o d < 13$ while modes LCP within $n_{eff} < 2.8$ and $k_o d < 11$. For Fig.7, RCP modes shown within $n_{eff} < 5.5$ and $k_o d < 6$ while LCP

modes are within $n_{eff} < 6$ and $k_o d < 5$. As a result, we can say that increasing the values of dielectric constants leads to a large effective refractive index n_{eff} within the less normalized frequency. It is worth mentioning that even modes do not provide any support for the zero mode for any parameters used, unlike odd modes, as shown in the figures. This change can vary depending on the specific waveguide design and material properties. The reason for this disappearance is complex and has to do with the interaction between the light wave, the chiral metamaterial properties, and the electrical properties of graphene. The graphene modifies the way the light interacts with the waveguide, leading to the absence of the fundamental mode.

VII. CONCLUSIONS

In conclusion, the results showed that graphene properties affect the propagation properties of light, which in turn causes the disappearance of the fundamental odd mode. The reason for this disappearance is the interaction between the light wave, the chiral metamaterial properties, and the electrical properties of graphene. The even modes do not provide any support for the fundamental mode for any parameters used. Increasing the dielectric constant values leads to a large effective refractive index n_{eff} with less normalized frequency. We can get the same value for effective refractive index n_{eff} within less normalized frequency $k_o d$ in the presence of graphene interfaces case. All modes begin with a backward propagation and turn into a forward propagation when increasing normalized frequency. Backward propagation is due to the presence of metamaterials, but this change in behavior occurs due to the influence of graphene. Moreover, it can be said that the refractive index for multilayered graphene decreases with increased thickness.

CONFLICT OF INTEREST

Authors declare that they have no conflict of interest.

REFERENCES

[1]N. Fawaz, and A. Hameed, "Wave Propagation in Dielectric Slab Waveguide with Two Different Cladding Materials," *Journal of University of Anbar for Pure Science*, Vol.7, No.1, 2013.

[2] Q. Cheng, T. Cui, and C. Zhang, "Waves in Planar Waveguide Containing Chiral Nihility Metamaterial," *Optics Communications*, Vol.276, No.2, pp.317-321, 2007.

[3] M. Baqir, and P. Choudhury, "Investigation of Uniaxial Anisotropic Chiral Metamaterial Waveguide with Perfect Electromagnetic Conductor Loading," *Optik*, Vol.126, pp.1228-1232, 2015.

[4] H. Salman, and H. Yasser, "Guided Modes in Slab Waveguide with Central Anisotropic Metamaterial Layer," *IOP Conf. Series: Materials Science and Engineering*, Vol.928, No.7, pp.072127, 2020.

[5]S. Shaddod, and H. Yasser, "Theoretical Study of Sensitivity of Slab-Sensor with Metamaterial," *University of Thi-Qar Journal*, Vol.14, No.1, 2019.

[6] I. Semchenko, S. Khakhomov, and S. Tretyakov, "Chiral Metamaterial with Unit Negative Refraction Index," *The European Physical Journal Applied Physics*, Vol.46, No.3, pp.32607, 2009.

[7] M. Baqir, and P. Choudhury, "On the Energy Flux Through a Uniaxial Chiral Metamaterial Made Circular Waveguide under PMC Boundary," *Journal of Electromagnetic Waves and Applications*, Vol.26, No.16, pp.2165-2175, 2012.

[8] A. Helal, S. Taya, and K. Elwasife, "Propagation of Electromagnetic Waves in Slab Waveguide Structure Consisting of Chiral Nihility Claddings and Negative-Index Material Core Layer," *Photonic Sensors*, Vol.8, No.2, pp.176-187, 2018.

[9]M. Abadla, and S. Taya, "Theoretical Investigation of Guided Modes in Planar Waveguides Having Chiral Negative Index Metamaterial Core Layer," *Optik - International Journal for Light and Electron Optics*, Vol.131, pp.562-573, 2016.

[10] J. Ctyroky, J. Petracek, P. Kwiecien, I. Richter, and V. Kuzmiak, "Graphene on an Optical Waveguide: Comparison of Simulation Approaches," *Optical and Quantum Electronics*, Vol.52, No.149, pp.1-14, 2020.

[11]H. Xiong, Q. Ji, T. Bashir, and F. Yang, "Dual-Controlled Broadband Terahertz Absorber Based on Graphene and Dirac Semimetal," *Optics Express*, Vol.28, No. 9, 2020.

[12] Z. Li, X. Shen, Y. Hua, X. Ruan, and Y. Dai, "Leaky Mode Transition and Enhanced Resonance in Tilted Fiber Bragg Grating," *Journal of Applied Physics*, Vol.126. No.154501, 2019.

[13] A. Boretti, L. Rosa, J. Blackledge, and S. Castelletto, "A Preliminary Study of a Graphene Fractal Sierpinski Antenna," *IOP Conf. Series: Materials Science and Engineering*, Vol.840, No.012003, 2020.

[14] K. Ooi, and D. Tan, "Nonlinear Graphene Plasmonics," *The Royal Society*, Vol.473, No.20170433, 2017.

[15] G. Jacob, and G. Raina, "Frequency Dependent Graphene Surface Plasmon Properties on Different Dielectrics," *International Journal of Recent Technology and Engineering*, Vol.8, pp.2277-3878, 2019.